

Superconducting properties and c -axis superstructure of $\text{Mg}_{1-x}\text{Al}_x\text{B}_2$

J. Y. Xiang, D. N. Zheng,* J. Q. Li, L. Li, P. L. Lang, H. Chen, C. Dong, G. C. Che, Z. A. Ren, H. H. Qi,[†] H. Y. Tian, Y. M. Ni, and Z. X. Zhao

National Laboratory for Superconductivity, Institute of Physics and the Center for Condensed Matter Physics, Chinese Academy of Sciences, Beijing 100080, People's Republic of China

(Received 20 April 2001; revised manuscript received 8 January 2002; published 17 June 2002)

The superconducting and structural properties of a series of $\text{Mg}_{1-x}\text{Al}_x\text{B}_2$ samples have been investigated. X-ray diffraction results confirmed the existence of a structural transition associated with a significant change in interboron layer distance as reported previously by Slusky *et al.* Moreover, transmission-electron-microscopy observations revealed the existence of a superstructure with doubled lattice constant along the c -axis direction. We propose that this superstructure is probably related to the structural transition. The modifications of the superconducting transition temperature T_c , the normal-state resistivity, and the upper critical field $B_{c2}(0)$ by Al doping are discussed in terms of Al-substitution-induced changes in the electronic structure at the Fermi energy.

DOI: 10.1103/PhysRevB.65.214536

PACS number(s): 74.60.Ec, 74.62.Dh

I. INTRODUCTION

The discovery of superconductivity in magnesium diboride with a transition temperature T_c of 39 K has attracted considerable interest.¹ This is because this metallic binary compound, which has been known since 1953,² consists of no transition metals and yet exhibits a remarkably high transition temperature, higher than the value obtained in any other metallic binary compounds. MgB_2 adopts a very simple hexagonal crystal structure, comprising interleaved two-dimensional boron and magnesium layers.² The appearance of superconductivity in MgB_2 with such a high value of T_c immediately raises the speculation for even higher superconducting temperatures in conventional metallic binary materials. On the other hand, the underlying mechanism of superconductivity in this compound is still an issue of current debate. There are mainly two competitive theories of superconductivity in MgB_2 . The first one is based on the well-established phonon-mediated BCS theory,³ and the high T_c value is believed to be due to the high phonon frequencies and strong electron-phonon interactions. This theory is supported by the results of a number of different experiments such as isotope effect,⁴ quasiparticle tunneling,^{5,6} specific heat,⁷ photoemission spectroscopy,⁸ and inelastic neutron scattering.⁹ The second theory concerning the superconductivity in MgB_2 was put forward by Hirsch^{10,11} who proposed a “universal” mechanism where superconductivity in MgB_2 was driven by the paring of dressed holes. Indeed, the hole character of the carriers in MgB_2 was confirmed by Hall measurements.¹²

Soon after the discovery of superconductivity in MgB_2 , Slusky *et al.*¹³ reported studies of how the behavior responds to the substitution of Al for Mg in this compound. They observed that T_c decreases smoothly by a few degrees with increasing x for $0 \leq x < 0.1$ and bulk superconductivity disappears completely due to a structural instability for $x > 0.1$. In this paper, the effect of partial Al substitution for Mg on the structural and superconducting properties of MgB_2 is studied. In particular we have observed a superstructure in Al-

doped samples. We suggest that this superstructure is related to the structural transition reported by Slusky *et al.*¹³ The superconducting transition temperature, normal-state resistivity, and upper critical field were also studied. The variation of these parameters with Al substitution concentration is discussed in connection with the change in the structure and the density of states at the Fermi energy.

II. EXPERIMENT

Polycrystalline samples used in this study were prepared by a conventional solid reaction process. Two series of samples with a similar fabrication process were made. Starting materials were elemental powders of Mg, Al, and B. The raw materials with nominal composition of $\text{Mg}_{1-x}\text{Al}_x\text{B}_2$ were well mixed and pressed into disks 8 mm in diameter and 0.4 g in weight. These disks were wrapped with Ta foil and sealed in quartz tubes under a background pressure about 10^{-3} Pa. The sealed quartz tubes under a background pressure about 10^{-3} Pa. The sealed quartz tubes were placed in a tube furnace, and the temperature was ramped at a rate of 100 °C per hour to 900 °C and held for 2 or 3 h. This was followed by furnace cooling to the room temperature.

The microstructures and phase purity of the samples were studied by means of x-ray diffraction (XRD) and transmission electron microscopy (TEM). For TEM examination, wafers of the samples were first metallographically polished and then thinned by ion milling. The local composition was probed by energy-dispersive x-ray spectroscopy (EDX).

Resistivity measurements were made on bar-shaped samples of approximate dimensions $6 \times 3 \times 2$ mm³ using a four-probe technique with a current of 10 mA. ac-susceptibility measurements were also performed to determine the superconducting transition temperature. dc magnetization was measured in a Quantum Design superconducting quantum interference device (SQUID) magnetometer.

III. RESULTS AND DISCUSSION

The x-ray powder diffraction patterns obtained on the samples showed that the predominant phase was of MgB_2

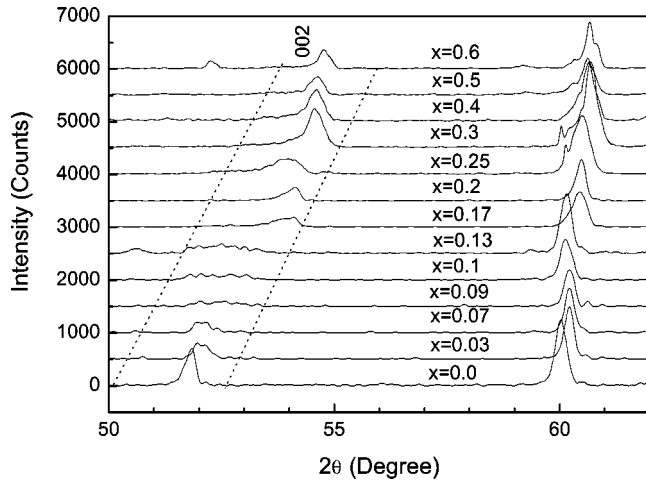


FIG. 1. Partial representation of x-ray diffraction patterns for a series of $\text{Mg}_{1-x}\text{Al}_x\text{B}_2$ samples.

type and there was some minor amount of impurity phases such as MgO presented in the samples. The partial representation of the XRD patterns in the 2θ range of 50° to 60° is shown in Fig. 1. The results are similar to that reported by Slusky *et al.*¹³; i.e., the substitution of Al results in a significant change in the c -axis lattice parameter while the in-plane lattice parameter is relatively constant. In the range approximately between $x=0.09$ to $x=0.25$, the (002) reflection peak becomes broad, indicating the partial collapse of the separation between boron sheets and the presence of two isostructure phases. Figure 2 shows the lattice parameters as a function of the Al substitution level. In the shadowed region, because of the peak broadening, there is a large uncertainty associated with the value of c . Nevertheless, the data in Fig. 2 show that in the shadowed region there appears a discontinuity, which could be related to a structural transition as pointed out in Ref. 13.

Resistivity measurements were carried out on two series

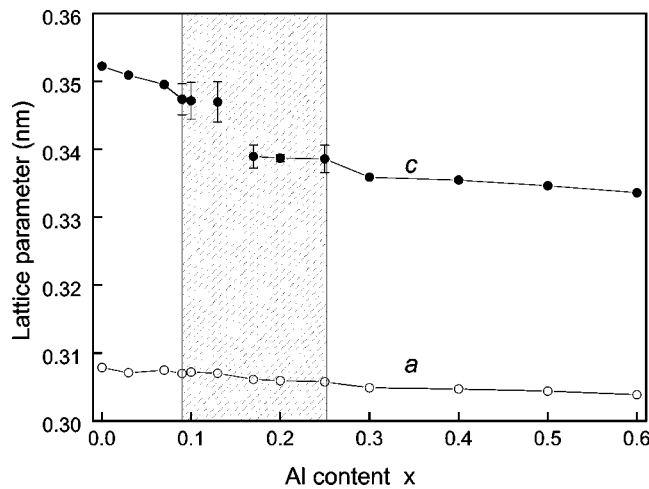


FIG. 2. The lattice parameter a and c as a function of Al concentration. In the shadowed region, the (002) reflection peak is broad, indicating the partial collapse of the separation between boron layers.

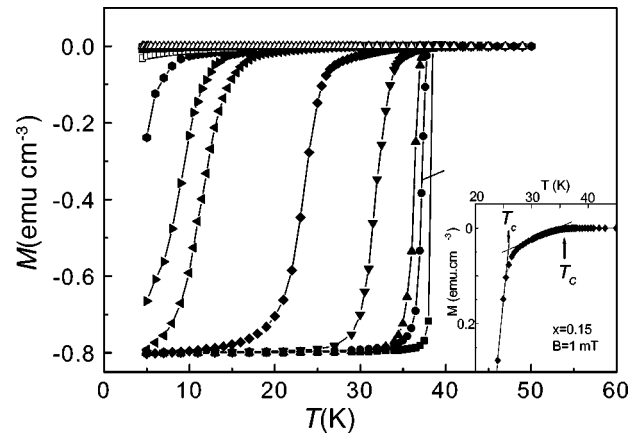


FIG. 3. Zero-field-cooled (ZFC) magnetization as a function of temperature for different Al doping levels. The inset is a magnified part of one of the transition curves to show the definition of $T_{c(\text{bulk})}$ and $T_{c(\text{onset})}$.

of samples that were fabricated under almost the same conditions (one was sintered at 900°C for 2 h and another one was at the same temperature for 3 h). The intention was to investigate how the normal-state resistivity varied with Al doping concentration. However, the data obtained did not show a clear trend of the variation for the resistivity with Al content over the whole doping range we investigated ($0 \leq x \leq 0.6$). In particular, there was no sharp rise in the resistivity around the phase transition around $x=0.1$ as would be observed in alloys of metals. There are a number of factors that could mask the intrinsic resistivity of the materials studied. These include sample density variation, grain boundary conditions, and disorder scattering. For the all samples measured, we checked the density and found that the values were around 70% of the theoretical ones while the variation between the samples was within 10%. Thus, the porosity of the samples would certainly affect the absolute resistivity values, but its effect on the relative variation of the resistivity might not be substantial. The resistivity is around $30 \mu\Omega \text{ cm}$ at 40 K for undoped samples.

Although the resistivity data were rather scatter and showed no clear trend with the increase of the Al level over the whole doping range, we found that in the low-doping region ($x < 0.1$) the normal-state resistivity increases monotonically for both series of samples we made. This is in agreement with the observation of Lorenz *et al.*¹⁴ The increase of the normal-state resistivity (at least within the doping level of 0.1) by Al doping is consistent with the hypothesis that the charge carrier in MgB_2 is hole like^{10,11} since the substitution of Al^{3+} for Mg^{2+} reduces the carrier density and subsequently leads to an increase in the normal-state resistivity. It has been suggested that conduction in MgB_2 occurs primarily in the B layer³ and thus the effect of Al doping on the Mg site on the impurity scattering is small while the effect of charge transfer is more significant. The results reported in Ref. 14 also showed an increase in thermopower in Al-doped samples, indicating the reduction of carrier numbers.

In Fig. 3, we illustrate the evolution of the superconduct-

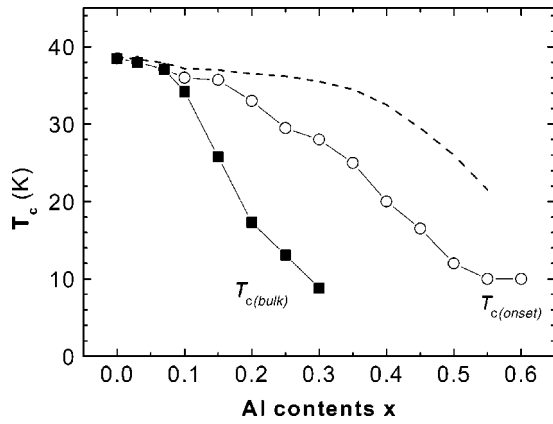


FIG. 4. Variation of the onset superconducting transition temperature $T_{c(onset)}$ and bulk superconducting transition temperature $T_{c(bulk)}$ with Al doping level. Due to the rounded curvature between $T_{c(bulk)}$ and $T_{c(onset)}$, there is a large error bar associated with $T_{c(onset)}$. The curve of $T_{c(onset)}$ (open circles) defined in Fig. 3 might be regarded as the lower bound while the dashed line is the upper bound of $T_{c(onset)}$.

ing transition with Al doping in $Mg_{1-x}Al_xB_2$ by presenting a series of zero-field-cooled magnetization versus temperature curves measured on samples with a variety of different doping levels. The measurements were carried out on bar-shaped samples. At the low-doping level, the transition is sharp and the transition decreases slightly with an increase of the Al doping level. As the Al concentration increases, the transition becomes broad and there appear two transitions as indicated in the graph. We believe that the first transition is the transition within grains while the second one is associated with the establishment of bulk screening currents. For doping levels lower than $x=0.3$, the full diamagnetism signal is obtained whereas at higher-doping levels the bulk superconductivity disappears. Furthermore, in the high doping region ($x > 0.3$), not only the bulk superconductivity disappears, but also the diamagnetism magnetization becomes smaller and smaller. This is attributed to the decreased superconducting volume fraction within grains in the Al-doped samples resulting from the appearance of a nonsuperconducting phase.¹³

In Fig. 4, we show the variation of superconducting transition temperature as a function of Al substitution level. In the graph we present the data of both the onset superconducting transition temperature $T_{c(onset)}$ and the bulk transition temperature $T_{c(bulk)}$. The determination of these two characteristic temperatures is illustrated in the inset of Fig. 3. Because the magnetization data in the temperature range between $T_{c(onset)}$ and $T_{c(bulk)}$ show rounded curvature, there is a large uncertainty associated with $T_{c(onset)}$. Therefore the value in Fig. 3 (open circles) might be regarded as the lower bound of $T_{c(onset)}$. The dashed line in the graph represents the upper bound. For samples with $x > 0.4$, there is still a very small but measurable diamagnetism signal. In the low-doping region the two transition temperatures are close and decrease slowly with increasing Al doping level. For doping levels above $x=0.1$, $T_{c(bulk)}$ drops more quickly than $T_{c(onset)}$. The $x=0.1$ composition coincides approximately with the substitution level at which the two-phase region

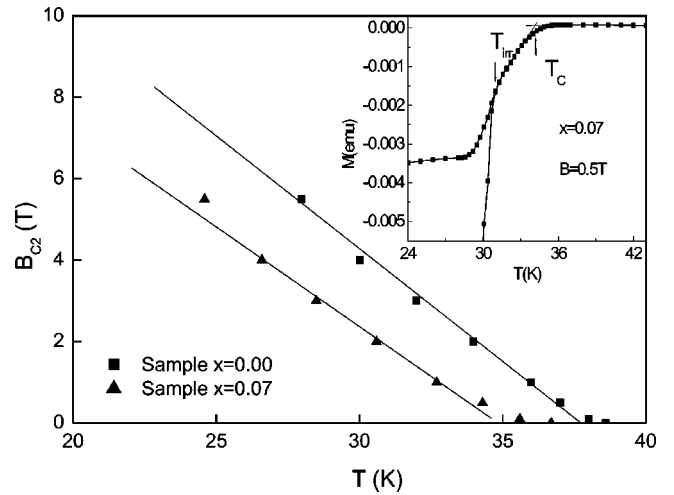


FIG. 5. Temperature dependence of the upper critical field $B_{c2}(0)$ for the $x=0$ and 0.07 samples. The inset shows the FC and ZFC magnetization data as a function of temperature measured at 0.5 T for the $x=0.07$ sample. The superconducting transition temperature T_c and the irreversibility temperature T_{irr} are indicated in the graph.

appears. As pointed out by Slusky *et al.*,¹³ the compound MgB_2 is near a structural instability, at slightly higher electron concentration, which can destroy the superconductivity. Their experimental results and the results presented here suggested that the suppression of bulk superconductivity occurs at the same Al doping level at which a structural transition occurs. After the structural transition, a presumably nonsuperconducting phase appears, and the two phases are intergrown on a nanometer-length scale. Hence the granular nature of the superconducting phase and proximate effects, caused by the intergrowth, together with the possible nonuniform distribution of Al contents is expected to influence the shapes of the curves in Fig. 3 and the T_c dependence in Fig. 4.

On the other hand, the decrease of T_c at substitution levels lower than $x=0.1$ has been attributed to a density-of-states effect.^{13,14} In MgB_2 the Fermi energy E_F is close to an edge of rapidly decreasing density of states and any increase of E_F by Al substitution could result in a significant decrease of the density of states at the Fermi energy $N(E_F)$, which, in the BCS formalism, leads to a decrease of T_c . In the next few paragraphs, we present the results of the upper critical field $B_{c2}(0)$ and try to deduce some information concerning $N(E_F)$.

In the inset of Fig. 5 the magnetic moment versus temperature curve measured at 0.5 T for the $x=0.07$ sample is shown. A small normal-state background contribution has been subtracted from the data. As commonly observed in high- T_c superconductors, there were two characteristic temperatures T_c and T_{irr} . In the region between these two temperatures, field-cooled (FC) and zero-field-cooled (ZFC) magnetization data were overlapped. The superconducting transition temperature was defined as the intercept of a linear extrapolation of the magnetic moment in the superconducting state with the normal-state base line. The field dependence of T_c gives the upper critical field $B_{c2}(0)$ data, which

are presented in Fig. 5 for the two samples with $x=0$ and $x=0.07$, respectively. For both samples, $B_{c2}(0)$ shows an approximately linear temperature dependence with a slope of -0.6 T/K and -0.58 T/K, respectively. For the $x=0$ sample, the value is similar to that reported in the literature.¹⁵

The relation between the zero-temperature upper critical field $B_{c2}(0)$ and dB_{c2}/dT at T_c is^{16,17}

$$B_{c2}(0) = 0.5758 \left(\frac{\kappa_1(0)}{\kappa} \right)_{T_c} \left(\frac{dH_{c2}}{dT} \right)_{T_c}. \quad (1)$$

In the dirty limit $\kappa_1(0)/\kappa = 1.20$,^{18,19} while in the clean limit $\kappa_1(0)/\kappa = 1.26$.²⁰ These expressions yield $B_{c2}(0) = 16.2$ T for $x=0$ and $B_{c2}(0) = 14.8$ T for $x=0.07$, respectively, assuming the dirty limit. Similarly, we obtain $B_{c2}(0) = 16.8$ T for $x=0$ and $B_{c2}(0) = 15.4$ T for $x=0.07$, respectively, assuming the clean limit. Clearly, the decrease of $B_{c2}(0)$ is primarily due to the decrease of T_c and the slope is barely changed. The coherent length at zero temperature, $\xi(0)$, may be estimated using the expression $B_{c2}(0) = \phi_0/2\pi\xi^2(0)$. For the undoped MgB₂ sample the value is $\xi(0) = 4.5$ nm in the dirty limit and $\xi(0) = 4.4$ nm in the clean limit.

The coherence length we just calculated is the Ginzburg-Landau (GL) coherence length. In order to know whether the samples are in the clean limit or in the dirty limit, we need to compare the BCS coherence length ξ_0 and the electronic mean free path l . The former can be estimated using the relation²¹ $\xi_0 = 0.15\hbar v_F/k_B T_c$, where v_F is the Fermi velocity. Taking an average value³ of $v_F = 4.7 \times 10^7$ cm/s, we obtain $\xi_0 = 14$ nm. On the other hand, for estimating l , we use the carrier density 6.7×10^{22} cm⁻³ (two carriers per unit cell) (Ref. 22) and the resistivity value of $30 \mu\Omega$ cm for our undoped MgB₂ sample. Then, l is estimated to be approximately 1 nm. This clearly puts the sample in the dirty limit. However, since the sample porosity and other extrinsic factors would certainly result in overestimated resistivity values, we should be cautious with the value of l . Canfield *et al.*²² reported very low resistivity values on dense MgB₂ wires and subsequently a long mean free path, and the clean limit behavior was inferred. The resistivity value reported in the literature varies greatly for MgB₂. We note that even for high-quality epitaxial thin-film samples resistivity values^{23,24} are about one order of magnitude higher than those reported in Ref. 22. In particular, the recent work by Eom *et al.*²⁵ and Patnaik *et al.*²⁶ has shown that oxygen could be alloyed onto B site which leads to a significant increase in resistivity and the upper critical field. Therefore, it is plausible that with increasing sample resistivity MgB₂ may change from the clean limit to the dirty limit. Furthermore, the data obtained on our MgB₂ samples show that the GL coherence length $\xi(0)$ is substantially shorter than the BCS coherence length ξ_0 , an indication of dirty limit behavior.

In assuming the dirty limit, we may infer some information about the density of states from the upper critical field data. As discussed above, the band calculation showed that in MgB₂ the Fermi energy is situated around a peak in the density of states.^{3,27,28} The substitution of Al increases the

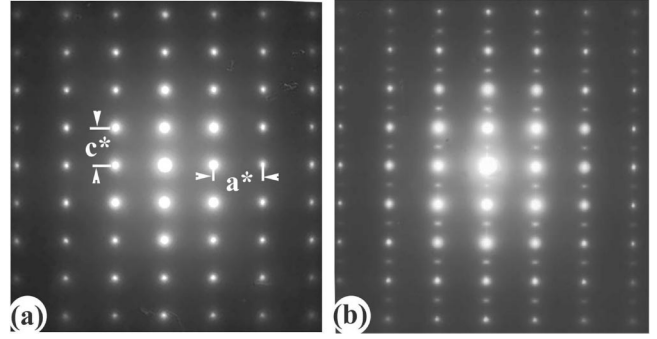


FIG. 6. TEM diffraction patterns for the two Mg_{1-x}Al_xB₂ samples. (a) $x=0$, (b) $x=0.25$.

electron transfer from the Mg plane. In a rigid band picture, this would mean a decrease of the density of states at the Fermi energy $N(E_F)$. In the dirty limit, $N(E_F)$ can be related to the slope of B_{c2} near T_c with the relation $-dB_{c2}/dT|_{T_c} \sim \rho N(E_F)$, where ρ is the residual normal-state resistivity. Clearly, the slight decrease of dB_{c2}/dT and the increase in the normal-state resistivity indicate that $N(E_F)$ is indeed reduced in the Al-doped sample. If the resistivity could be determined more accurately, a more quantitative estimation of (E_F) could be made.

In conventional alloy and intermetallic-compound superconductors such as NbTi and (Nb,Ti,Ta)₃Sn, the upper critical field $B_{c2}(0)$ can be increased by substitutional alloying which results in resistivity increases while having a much more mild effect on T_c and density of states. This can be illustrated by the direct dependence of $B_{c2}(0)$ on the normal-state resistivity through the formula²⁹ $B_{c2}(0) = 3.110\rho\gamma T_c$ (in SI units). Here γ is the electronic specific heat coefficient. The work by Eom *et al.*²⁵ and Patnaik *et al.*²⁶ appears to suggest that oxygen could be alloyed into MgB₂ on the B site and lead to a dramatic increase in the upper critical field even though T_c is reduced slightly.²⁵ In contrast the data shown here indicate that although low-level Al doping can increase the normal-state resistivity substantially in MgB₂ both $B_{c2}(0)$ and T_c are reduced. This is direct evidence that the rise in ρ is compensated for by the decrease in the density of states.

In order to characterize the structural features associated with the structural transition as reported in the present system, we have carried out TEM investigations on Al-doped samples, especially, with x ranging from 0.1 to 0.25. As a result, a variety of structural phenomena have been revealed in these materials, such as the phase separation and intergrowth of two structural phases. The most striking structural feature found in this investigation is the presence of a superstructure phase of doubled lattice parameter along the c -axis direction. Figure 6 presents the electron diffraction patterns for two samples taken along the b -axis direction. Figure 6(a) is the electron diffraction pattern of the pure MgB₂ sample; all diffraction spots can be well indexed by the hexagonal cell with lattice parameters of $a = 3.07$ Å and $c = 3.57$ Å. The pattern in Fig. 6(b) was taken on an $x = 0.25$ sample. In addition to the basic reflection spots, evident superstructure spots can be clearly recognized at the systematic $(h, k, l$

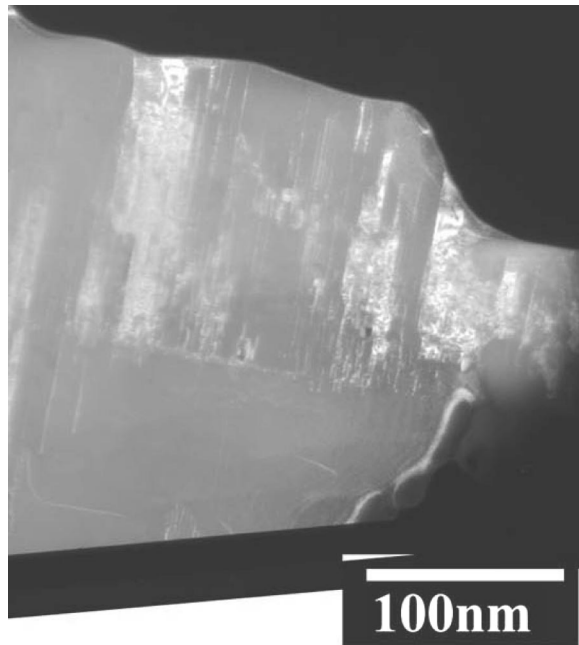


FIG. 7. A dark-field image of a grain for the $x=0.25$ sample.

+1/2) positions. TEM examination also revealed that the grains were very small, on the order of $0.1 \mu\text{m}$ in the $x=0.25$ sample. In Fig. 7, we show a dark-field image of a grain for the $x=0.25$ sample. We could see that the phase with the superstructure intergrows with the normal MgB_2 phase. A more detailed TEM study was performed subsequently and the results are reported elsewhere.³⁰ In particular, the results showed that the observed superstructure is a generic feature resulting from Al substitution in MgB_2 and that the superstructure is of MgAlB_4 structure with Mg layers and Al layers sitting alternately in the crystal lattice.

The superstructure, however, was not observed in XRD spectra. In principle, the appearance of the superstructure with doubled c -axis parameter would result in an additional (00 l) peak at low 2θ angle. The XRD data showed no sign of such a peak within the instrumental sensitivity. We propose that this is due to the very similar x-ray scattering factor for Mg and Al atoms. The diffraction of x rays by atoms in a

crystal lattice is due to the interaction between the surrounding electrons and x rays. Mg and Al are elements that occupy positions next to each other in the periodic table, and the electron cloud distribution is very similar for Mg^{2+} and Al^{3+} . Therefore the scattering factor is almost the same for the two elements. Furthermore, the phase with superstructure is presented in small regions, especially for the low-Al-doped samples, and hence the XRD peak may smear and become difficult to observe. On the other hand, TEM can probe the structure in a comparatively small region. Moreover, the diffraction of charged electrons is more sensitive to the electric field potential of atoms, which are different for Mg and Al atoms. Thus, the superstructure can be observed more readily by TEM.

In summary, we have investigated the effect of Al substitution for Mg on the structural and superconducting properties of $\text{Mg}_{1-x}\text{Al}_x\text{B}_2$ samples. The x-ray diffraction results confirmed the existence of a structural transition associated with the significant change in interboron layer distance as reported previously by Slusky *et al.*¹³ Moreover, a transmission electron microscopy examination showed the existence of a superstructure in the direction perpendicular to the boron honeycomb layers with doubled c -axis lattice parameter. We propose the observed superstructure be related to the structural transition. The experimental results showed that the normal-state resistivity was increased and T_c was decreased with increasing Al concentration, respectively. The upper critical field $B_{c2}(0)$ was determined for samples with low Al concentrations and found to be reduced by Al doping. Furthermore, an estimation of the density of states at the Fermi energy $N(E_F)$ using the $B_{c2}(0)$ and normal-state resistivity data suggests that $N(E_F)$ is decreased too, being consistent with theoretical calculations.

ACKNOWLEDGMENTS

This work was supported by the National Center for Research and Development on Superconductivity and the Ministry of Science and Technology Grant No. NKBRSG-19990646. One of us (J.Q.L.) acknowledges support of the “Hundred of Talents” program organized by the Chinese Academy of Sciences, China.

*Corresponding author. Electronic address: dzheng@ssc.iphy.ac.cn

[†]Also at College of Materials Science and Chemical Engineering, Yanshan University Qinghuangdao 066004, People’s Republic of China.

¹J. Nagamatsu, N. Nakagawa, T. Muranaka, Y. Zenitani, and J. Akimitsu, *Nature (London)* **410**, 63 (2001).

²J. E. Jones and R. E. Marsh, *J. Am. Chem. Soc.* **76**, 1434 (1954).

³J. Kortus, I. I. Mazin, K. D. Belashchenko, V. P. Antropov, and L. L. Boyery, *Phys. Rev. Lett.* **86**, 4656 (2001).

⁴S. L. Bud’ko, G. Lapertot, C. Petrovic, C. E. Cunningham, N. Anderson, and P. C. Canfield, *Phys. Rev. Lett.* **86**, 1877 (2001).

⁵H. Schmidt, J. F. Zasadzinski, K. E. Gray, and D. G. Hinks, *Phys. Rev. B* **63**, 220504 (2001).

⁶Amos Sharoni, Israel Felner, and Oded Millo, *Phys. Rev. B* **63**, 220508 (2001).

⁷R. K. Kremer, B. J. Gibson, and K. Ahn, cond-mat/0102432 (unpublished).

⁸T. Takahashi, T. Sato, S. Souma, T. Muranaka, and J. Akimitsu, *Phys. Rev. Lett.* **86**, 4915 (2001).

⁹T. Yildirim, O. Gulseren, J. W. Lynn, C. M. Brown, T. J. Udovic, H. Z. Qing, N. Rogado, K. A. Regan, M. A. Hayward, J. S. Slusky, T. He, M. K. Haas, P. Khalifah, K. Inumaru, and R. J. Cava, *Phys. Rev. Lett.* **87**, 037001 (2001).

¹⁰J. E. Hirsch, *Phys. Lett. A* **281**, 44 (2001).

¹¹J. E. Hirsch and F. Marsiglio, *Phys. Rev. B* **64**, 144523 (2001).

¹²W. N. Kang, C. U. Jung, H. P. Kim, Min-Seok Park, S. Y. Lee, Hyeong-Jin Kim, Eun-Mi Choi, Kyung Hee Kim, Mun-Seog Kim, and Sung-Ik Lee, *Appl. Phys. Lett.* **79**, 982 (2001).

¹³J. S. Slusky, N. Rogada, K. A. Regan, M. A. Hayward, P. Khalifah, T. He, K. Inumaru, S. M. Loureiro, M. K. Hass, H. W.

- Zandbergen, and R. J. Cava, *Nature (London)* **410**, 343 (2001).
- ¹⁴B. Lorenz, R. L. Meng, Y. Y. Xue, and C. W. Chu, *Phys. Rev. B* **64**, 052513 (2001).
- ¹⁵D. K. Finnemore, J. E. Ostenson, S. L. Bud'ko, G. Lapertot, and P. C. Canfield, *Phys. Rev. Lett.* **86**, 2420 (2001).
- ¹⁶A. L. Fetter and P. C. Hohenberg, in *Superconductivity*, edited by R. D. Parks (Dekker, New York, 1969), p. 817.
- ¹⁷B. Miihlschlegel, *Z. Phys.* **155**, 313 (1959).
- ¹⁸N. R. Werthamer, E. Helfand, and P. C. Hohenberg, *Phys. Rev.* **147**, 288 (1966).
- ¹⁹K. Maki, *Phys. Rev.* **148**, 362 (1966).
- ²⁰G. Eilenberger, *Phys. Rev.* **153**, 584 (1967).
- ²¹T. E. Faber and A. B. Pippard, *Proc. R. Soc. London, Ser. A* **231**, 336 (1955).
- ²²P. C. Canfield, D. K. Finnemore, S. L. Bud'ko, J. E. Ostenson, G. Lapertot, C. E. Cunningham, and C. Petrovic, *Phys. Rev. Lett.* **86**, 2423 (2001).
- ²³W. N. Kang, Hyeong-Jin Kim, Eun-Mi Choi, C. U. Jung, and Sung-Ik Lee, *Science* **292**, 1521 (2001).
- ²⁴W. N. Kang, Hyeong-Jin Kim, Eun-Mi Choi, Kijoon H. P. Kim, and Sung-Ik Lee, *Phys. Rev. B* **65**, 134508 (2001).
- ²⁵C. B. Eom, M. K. Lee, J. H. Choi, L. J. Belenky, X. Song, L. D. Cooley, M. T. Naus, S. Patnaik, J. Jiang, M. Rikel, A. Polyanskii, A. Gurevich, X. Y. Cai, S. D. Bu, S. E. Babcock, E. E. Hellstrom, D. C. Larbalestier, N. Rogado, K. A. Regan, M. A. Hayward, T. He, J. S. Slusky, K. Inumaru, M. K. Hass, and R. J. Cava, *Nature (London)* **441**, 558 (2001).
- ²⁶S. Patnaik, L. D. Cooley, A. Gurevich, A. A. Polyanskii, J. Jiang, X. Y. Cai, A. A. Squitieri, M. T. Naus, M. K. Lee, J. H. Choi, L. Belenky, S. D. Bu, J. Letteri, X. Song, D. G. Schlom, S. E. Babcock, C. B. Eom, E. E. Hellstrom, and D. C. Larbalestier, *Supercond. Sci. Technol.* **14**, 359 (2001).
- ²⁷D. R. Armstrong and P. G. Perkins, *J. Chem. Soc., Faraday Trans. 1* **275**, 13 (1979).
- ²⁸A. L. Ivanovskii and I. Medvedeva, *Russ. J. Inorg. Chem.* **45**, 1234 (2000).
- ²⁹T. P. Orlando, E. J. McNiff, Jr., S. Foner, and M. R. Beasley, *Phys. Rev. B* **19**, 4545 (1979).
- ³⁰J. Q. Li, L. Li, F. M. Liu, C. Dong, J. Y. Xiang, and Z. X. Zhao, *Phys. Rev. B* **65**, 132505 (2002).